Journal of Anatomy

J. Anat. (2014) **225**, pp19–30 doi: 10.1111/joa.12194

Morphological integration in the forelimb of musteloid carnivorans

Anne-Claire Fabre,[1] Anjali Goswami,[2] Stéphane Peigné[3] and Raphaël Cornette[4]

[1]*Department of Evolutionary Anthropology, Duke University, Durham, NC, USA*
[2]*Department of Genetics, Evolution, and Environment and Department of Earth Sciences, University College London, London, UK*
[3]*CR2P–UMR 7207 CNRS/MNHN/Univ Paris 06, Paris, France*
[4]*OSEB–UMR 7205 CNRS/MNHN, Paris, France*

Abstract

The forelimb forms a functional unit that allows a variety of behaviours and needs to be mobile, yet at the same time stable. Both mobility and stability are controlled, amongst others, at the level of the elbow joint. This joint is composed of the humero-ulnar articulation, mainly involved during parasagittal movements; and the radio-ulnar articulation, mainly allowing rotation. In contrast, the humero-radial articulation allows both movements of flexion–extension and rotation. Here, we study the morphological integration between each bone of the forelimb at the level of the entire arm, as well as at the elbow joint, in musteloid carnivorans. To do so, we quantitatively test shape co-variation using surface 3D geometric morphometric data. Our results show that morphological integration is stronger for bones that form functional units. Different results are obtained depending on the level of investigation: for the entire arm, results show a greater degree of shape co-variation between long bones of the lower arm than between the humerus and either bone of the lower arm. Thus, at this level the functional unit of the lower arm is comprised of the radius and ulna, permitting rotational movements of the lower arm. At the level of the elbow, results display a stronger shape co-variation between bones allowing flexion and stability (humerus and ulna) than between bones allowing mobility (ulna and radius and humerus and radius). Thus, the critical functional unit appears to be the articulation between the humerus and ulna providing the stability of the joint.

Key words: 3D geometric morphometrics; Carnivora; co-variation; elbow; functional morphology; Musteloidea.

Introduction

The relationships between the long bones of the forelimb in quadrupedal animals and their functional role have been a subject of considerable interest. The morphology of the forelimb has been suggested to be a good indicator of locomotor ecology and other behaviours, such as foraging, mating, grasping and grooming (Ewer, 1973; Gonyea, 1978; Rose, 1988, 1993; MacLeod & Rose, 1993; Iwaniuk et al. 1999; Argot, 2001, 2003; Andersson, 2003, 2004, 2005; Andersson & Werdelin, 2003; Schutz & Guralnick, 2007; Candela & Picasso, 2008; Flores & Diaz, 2009; Steiner-Souza et al. 2010; Halenar, 2011). The forelimb is composed of three long bones, with the humerus forming the upper arm, and the ulna and radius composing the lower arm. The humerus shares its distal articulation with the proximal part of both the ulna and the radius (Fig. 1). Both mobility and stability of the forelimb are controlled at the level of the elbow joint. This joint includes three articulations: the humero-ulnar; the humero-radial; and the proximal radio-ulnar articulation. It is composed of two articulations mainly involved in only one function: (i) the humero-ulnar joint, which is involved during movements along one axis (flexion and extension); and (ii) the radio-ulnar joint, which is a pivot joint allowing rotation of the radius about the ulna (Argot, 2001). In contrast, the humero-radial articulation allows both movements of flexion–extension and rotation (pronation–supination), with the radial head turning on the capitulum of the humerus (Rose, 1988, 1993; MacLeod & Rose, 1993; Argot, 2001, 2003; Patel, 2005).

Previous studies have mainly focused on the relationship between elbow morphology and locomotor mode (Andersson, 2003, 2004, 2005; Milne et al. 2009; Steiner-Souza et al. 2010; Halenar, 2011), but have largely ignored

Correspondence
Anne-Claire Fabre, Animal Locomotion Laboratory, Department of Evolutionary Anthropology, Duke University, Campus Box 90383, Durham, 27708 NC, USA. T: +1 919-660-7348; F: +1 919-660-7348; E: aof3@duke.edu

Accepted for publication *31 March 2014*
Article published online *16 May 2014*

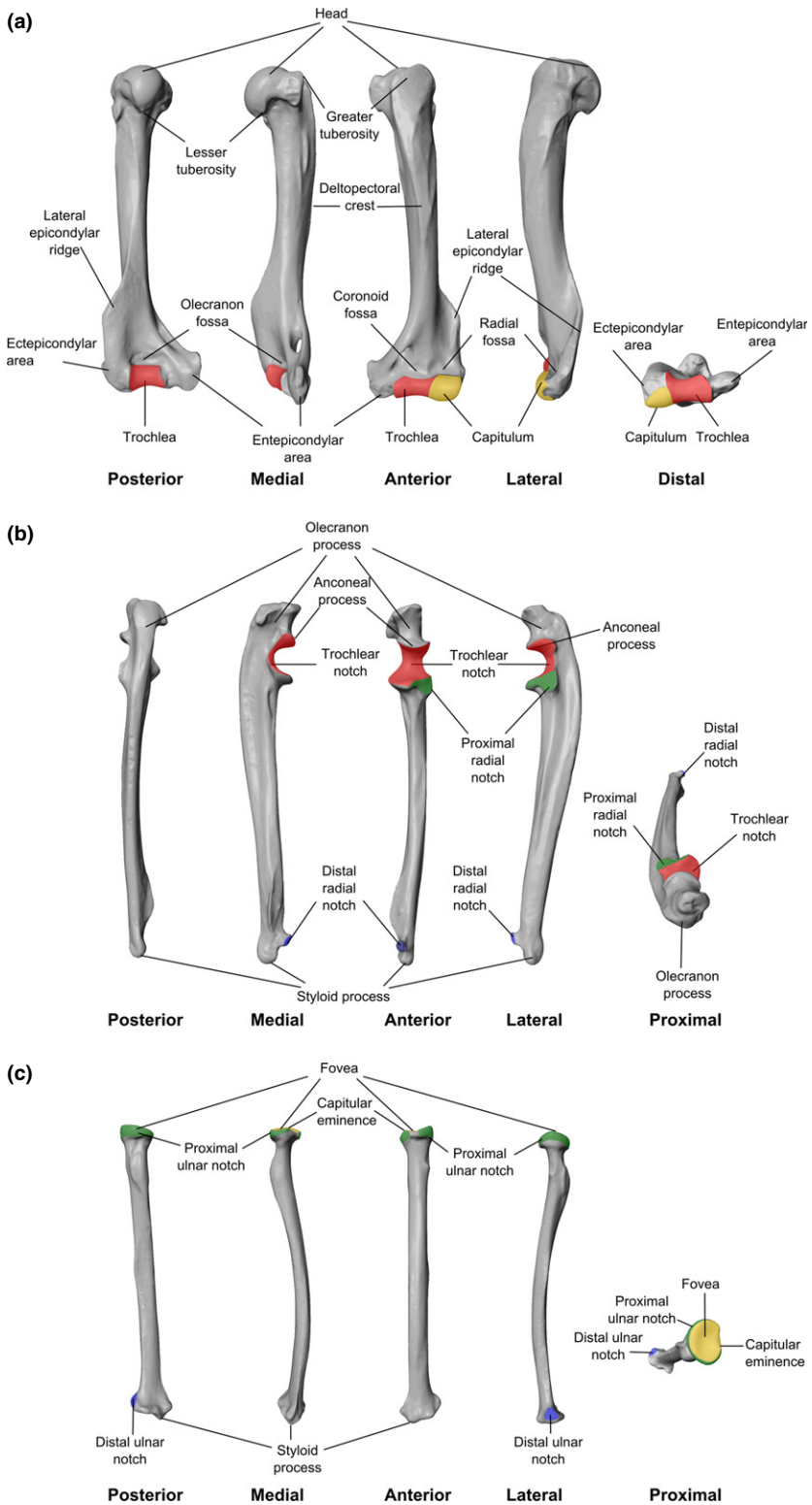

Fig. 1 Figure illustrating the anatomy of long bones of the forelimb. (a) Humerus, views from left to right: posterior, medial, anterior, lateral, distal; (b) ulna, views from left to right: posterior, medial, anterior, lateral, proximal; (c) radius, views from left to right: posterior, medial, anterior, lateral, proximal. Red surfaces represent the humero-ulnar joint; yellow surfaces represent the humero-radial joint; green surfaces represent the proximal radio-ulnar joint; and blue surfaces represent the distal radio-ulnar joint.

other aspects of the long bones and their interrelationships. Yet, all elements are crucial to ensure effective movement of the forelimb. The forelimb forms a functional unit that allows a variety of behaviours, and consequently selection will operate on the whole rather than on each bone separately (Cheverud, 1982), even if each long bone of the forelimb has a distinct developmental origin (Wellik & Capecchi, 2003; Young & Hallgrímsson, 2005; Goswami

et al. 2009; Schmidt & Fischer, 2009; Young et al. 2010; Bell et al. 2011; Bennett & Goswami, 2011; Fig. 2). The interactions between the elements of the forelimb have the potential to generate co-variations and correlations between the shape of each long bone, which can be defined as morphological integration (*sensu stricto*; Olson & Miller, 1958; Klingenberg, 2008, 2009; Hallgrímsson et al. 2009). Following its definition, morphological integration encompasses a common development and/or function of a morphological unit that produces co-variation among the composing elements (Olson & Miller, 1958; Schmidt & Fischer, 2009; Goswami & Polly, 2010). Developmental integration refers to the developmental influences shared between elements (Fig. 2) that may then shape the co-variation structure. Functional integration refers to the physical interaction of different elements needed to perform a functional task (e.g. a movement or a behaviour).

Here, we study the morphological integration between each long bone of the forelimb in musteloid carnivorans. The Musteloidea are a good model group because they display a great diversity of species comprising more than one-third of the total diversity of the Carnivora with a wide range of body sizes with little or no change in limb posture (Nowak, 2005; Wilson & Mittermeier, 2009; Fabre et al. 2013a,b). Furthermore, they are ecologically diverse, with a remarkable diversity of locomotor behaviours that ranges from aquatic species, such as the sea otter (*Enhydra*), over arboreal species such as the kinkajou (*Potos*), the olingo (*Bassaricyon*) and the red panda (*Ailurus*), semi-fossorial species such as the wolverine (*Gulo*), the badger (*Meles*) and some skunks (*Mephitis*, *Spilogale* and *Mydaus*), to semi-arboreal ones such as the raccoon, the tayra (*Eira*) and the coati (*Nasua*). Even if musteloids show a wide range of locomotor behaviours, it is important to note that there are no cursorial species in the group. Indeed, this absence of cursorial adaptation means that none of them has lost the ability to supinate their paws in contrary to carnivores such as canids and some hyaenids (Ewer, 1973; Andersson & Werdelin, 2003; Andersson, 2004; Van Valkenburgh, 2007). In addition, the diversity of locomotor behaviours observed in each clade suggests that they have colonized the same type of habitats and acquired the behavioural traits of interest independently (Sato et al. 2009, 2012; Eizirik et al. 2010). Finally, their phylogenetic relationships are well resolved (Sato et al. 2009, 2012; Eizirik et al. 2010).

To test and visualize shape co-variation and the degree of morphological integration, we used 3D landmark configurations describing the shape of the long bones of the forelimb, and more particularly their articulation. To test for shape co-variation we used two-block partial least square (2B-PLS) methods (Rohlf & Corti, 2000) performed on 3D geometric morphometric data. This allows us to test if there is shape co-variation between each of the long bones of the forelimb as a whole, as well as their articulations. Moreover, this allows us to investigate the degree of morphological integration between each bone and each part of the articulation of the elbow joint.

We predict co-variation and functional integration between the elements of the forelimb given their interactions during crucially important behaviours, such as locomotion or feeding. Furthermore, whereas the ulna and radius share two articulations, they share only one articulation with the humerus. In addition, the radius and ulna must interact during pronation and supination movements, which are important during locomotion and other behaviours (such as grasping, digging, prey capture and grooming). Consequently, we predict that there will be a greater degree of shape co-variation and morphological

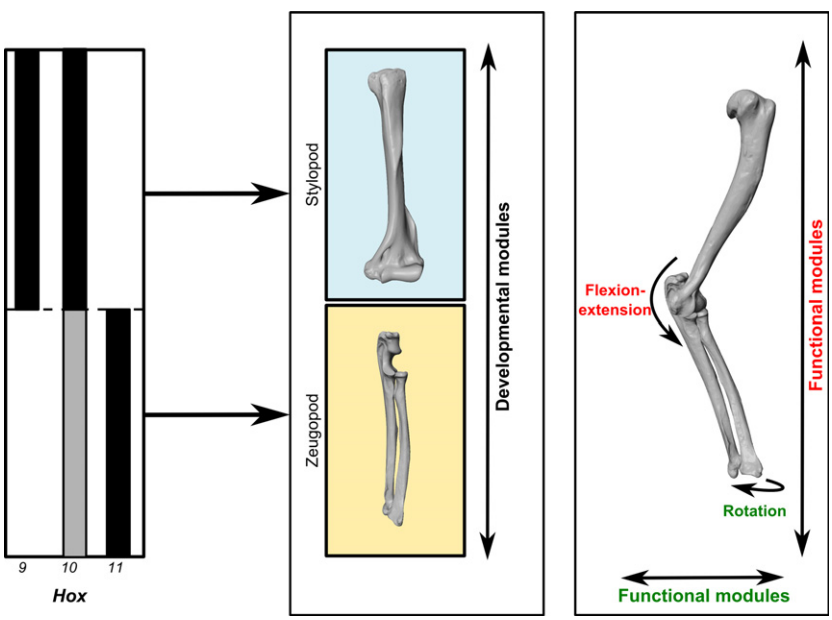

Fig. 2 Schematic representation of the developmental expression of *5′ Hox paralogous 9–13* involved in the proximo-distal patterning of forelimb in mice (modified from Wellik & Capecchi, 2003; Young & Hallgrímsson, 2005; Schmidt & Fischer, 2009; Young et al. 2010) showing in the first box the developmental modules: the blue box represents the humerus module and the yellow box represents the ulna and radius module; the second box represents functional modules involved in movements of rotation (green) and flexion–extension (red). Primary expression pattern is shown in black; lesser expression is shown in grey.

integration between the long bones of the lower arm (i.e. co-variation between the entire radius and ulna) than between the humerus and either bone of the lower arm (i.e. co-variation between the humerus and radius or humerus and ulna). When focusing on the elbow joint only, our predictions are different. The elbow joint is a synovial articulation that is under strong functional constraints. The ulna is tightly imbricate with the distal articulation of the humerus, and together they play an important role in the stability of the elbow. Thus, we predict that the shape co-variation between bones allowing stability in addition to mobility (co-variation between humerus and ulna) will be greater than between bones, assuring principally pronation–supination (co-variation between ulna and radius or co-variation between humerus and radius).

Materials and methods

Materials

Long bones of the forelimb (humerus, ulna and radius) of 77 individuals belonging to eight species of procyonids, one species of ailurid, four mephitids and 19 mustelids were used in our study. The number of specimens for each species ranged from one to five individuals (Table 1). For each specimen, each long bone belonged to the same forelimb (i.e. right or left). All specimens were adults and predominantly of wild caught origin. Forelimb bones were obtained from the following collections: Mammifères et Oiseaux, Muséum National d'Histoire Naturelle, Paris, France; the Naturhistorisches Museum, Basel, Switzerland; the Harvard Museum of Comparative Zoology, Cambridge, MA, USA; and the Smithsonian National Museum of Natural History, Washington, DC, USA; see Table S1 for a complete list of the specimens used in the analyses. All the bones of the forelimb were digitized using a Breuckmann 3D surface scanner at the Muséum National d'Histoire Naturelle, Paris (white light fringe StereoSCAN^{3D} model with a camera resolution of 1.4 megapixels).

Table 1 Details of specimens used in analyses with species name, common name, family, number of individuals included (*N*).

Species	Common name	Family	*N*
Mephitis mephitis	Striped skunk	Mephitidae	3
Spilogale putorius	Eastern spotted skunk	Mephitidae	3
Conepatus chinga	Molina's hog-nosed skunk	Mephitidae	1
Mydaus javanensis	Sunda stink badger	Mephitidae	2
Ailurus fulgens	Red panda	Ailuridae	5
Taxidea taxus	American badger	Mustelidae	2
Mellivora capensis	Honey badger	Mustelidae	2
Vormela peregusna	Marbled polecat	Mustelidae	2
Poecilogale albinucha	African striped weasel	Mustelidae	1
Galictis vittata	Greater grison	Mustelidae	1
Pteronura brasiliensis	Giant otter	Mustelidae	1
Lontra felina	Marine otter	Mustelidae	1
Lutra lutra	European otter	Mustelidae	1
Enhydra lutris	Sea otter	Mustelidae	2
Neovison vison	American mink	Mustelidae	1
Mustela lutreola	European mink	Mustelidae	2
Mustela putorius	European polecat	Mustelidae	2
Mustela eversmanii	Steppe polecat	Mustelidae	1
Melogale moschata	Chinese ferret-badger	Mustelidae	1
Meles meles	Eurasian badger	Mustelidae	3
Eira barbara	Tayra	Mustelidae	1
Gulo gulo	Wolverine	Mustelidae	2
Martes foina	Stone marten	Mustelidae	3
Martes martes	Pine marten	Mustelidae	2
Potos flavus	Kinkajou	Procyonidae	5
Procyon cancrivorus	Crab-eating raccoon	Procyonidae	3
Procyon lotor	Northern raccoon	Procyonidae	5
Nasua narica	White-nosed coati	Procyonidae	4
Nasua nasua	South American coati	Procyonidae	4
Bassaricyon alleni	Allen's olingo	Procyonidae	3
Bassaricyon gabbii	Bushy-tailed olingo	Procyonidae	3
Bassariscus astutus	Ringtail	Procyonidae	5

Quantification of shape variation using 3D geometric morphometrics

Because of the complex shape of the long bones of the forelimb and more specifically their articulations, they cannot be correctly represented using traditional anatomical landmarks. Thus, a 3D sliding-semilandmark procedure (Bookstein, 1997; Gunz et al. 2005) was used to quantify forelimb morphology based on scanned specimens. With this procedure, sliding-semilandmarks on surfaces and curves are transformed into geometrically (i.e. spatially) homologous landmarks (Parr et al. 2012) that can be used to compare shapes. Semilandmarks are allowed to slide along the curves and surfaces that are predefined on each bone of each specimen while minimizing the bending energy (Bookstein, 1991; Gunz et al. 2009; Mitteroecker & Gunz, 2009) between a template and each object to measure (i.e. each long bone of the forelimb for each individual; see Bookstein, 1997; Gunz et al. 2005; Gunz & Mitteroecker, 2013). The bending energy is, following the definition of Mitteroecker & Gunz (2009) and Gunz et al. (2009), 'the amount of bending of a deformation between two landmark configurations as quantified by the Thin Plate Spline function'. Landmarks and curves were obtained using the software package Idav Landmarks (Wiley et al. 2005), while Edgewarp3D 3.31 (Bookstein & Green, 2002) was used to obtain the sliding-semilandmark positions.

In this procedure each specimen is first defined by homologous landmark coordinates, which consisted of 21 landmarks for the humerus (Fig. 3; Table 2), 19 landmarks for the ulna (Fig. 3; Table 3) and 13 landmarks for the radius (Fig. 3; Table 4; see also Fabre et al. 2013a,b). Based on the homologous landmarks, all the sliding-landmarks of the template are warped onto the new specimen while minimizing the bending energy. Next, the warped sliding-landmarks are projected onto the predefined curves and surfaces of the new specimen. The curves consist of the distal surfaces of the articulation of the humerus and the proximal and distal articulation surface of the radius and ulna (Fig. 3). Finally, spline relaxation must be performed. Both sliding and relaxation are repeated iteratively until the bending energy is minimized. At the end of this procedure, 303 landmarks (21 homologous landmarks and 282 sliding-landmarks) for the humerus, 165 landmarks (13 homologous landmarks and 152 sliding-landmarks) for the radius, and 330 landmarks (19 homologous landmarks and

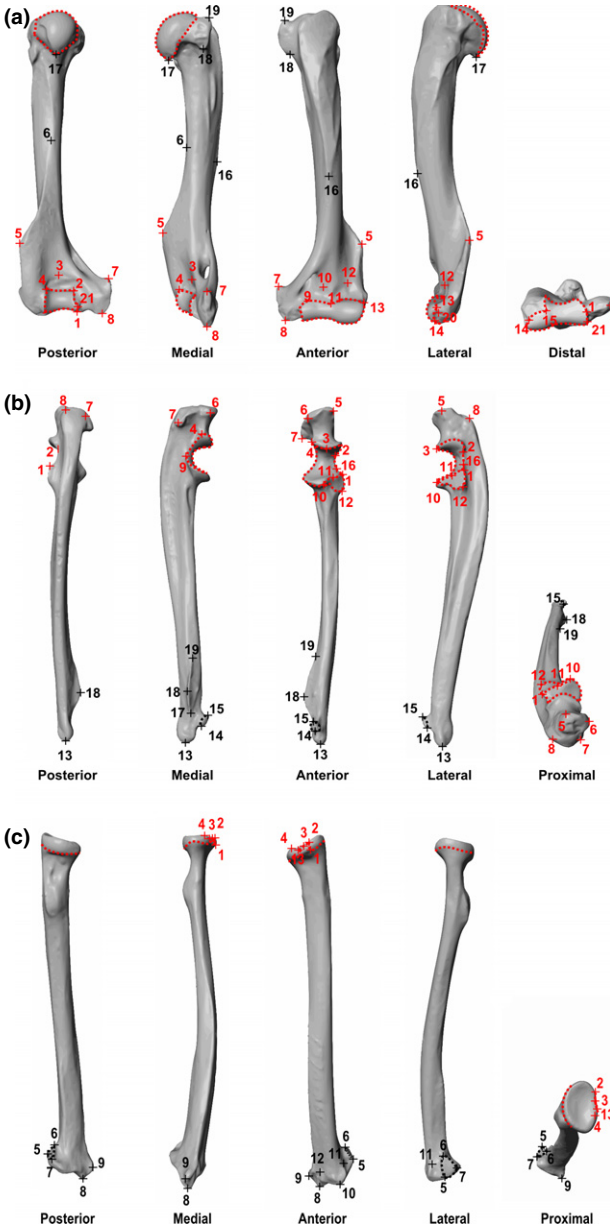

Fig. 3 Landmarks used in analyses to quantify shape variation on the forelimb bones. (a) Humerus; (b) ulna; (c) radius. Crosses represent landmarks used for the analyses at the level of the entire forelimb; red crosses represent landmarks used in the analyses at the level of the elbow; dashed-lines represent outlines used for the surface analyses at the level of the entire forelimb; red dashed-lines represent outlines used for the surface analyses at the level of the elbow articulation only.

311 sliding-landmarks) for the ulna are used to describe the shape of each bone and its articulations (proximal and distal). After this operation has been performed for each data set, the landmarks of all specimens can be compared using traditional geometric morphometric methods.

After the 3D sliding-semilandmark routine has been performed for each data set, the landmarks of all specimens can be compared using a generalized Procrustes superimposition (Rohlf & Slice, 1990),

Table 2 Definition of the landmarks of the humerus used for geometric morphometric analyses.

Landmark	Definition
1*	Most medial and distal point of the caudal part of the capitulum
2*	Most medial and proximal point of the caudal side of the capitulum
3*	Point of maximum of curvature of the olecranon fossa
4*	Most lateral and proximal point of the caudal side of the capitulum
5*	Point of maximum of convexity of the lateral epicondylar ridge
6	Point of insertion of the lateral epicondylar ridge on the diaphysis
7*	Most proximal tip of the entepicondylar area
8*	Most distal tip of the entepicondylar area
9*	Most medial and proximal point of the cranial side of the capitulum
10*	Point of maximum of curvature of the coronoid fossa
11*	Most proximal point of contact between the trochlea and the capitulum
12*	Point of maximum of curvature of the radial fossa
13*	Most lateral and proximal point of the cranial side of the capitulum
14*	Most distal and lateral point of the capitulum
15*	Most distal point of contact between the trochlea and the capitulum
16	Most distal point of the deltopectoral crest
17	Tip of the lesser tuberosity
18	Most proximal and medial point of the lesser tuberosity
19	Most distal and medial point of the lesser tuberosity
20*	Most lateral and distal point of the cranial side of the capitulum
21*	Point of maximum of concavity of the caudo-medio-distal part of the capitulum

*Represents landmarks used for the surface analyses of the elbow articulation.

which was performed on the point coordinates using the package Rmorph (Baylac, 2012) in R (R Development Core Team, 2012).

In the present study, this procedure was performed for four data sets (Fig. 3; Tables 2–4) to test if there is shape co-variation between each long bone of the forelimb as a whole, as well as the elbow articulation. The four data sets are composed of the entire data set at each level of investigation in addition to a subsampled data set that allows us to test the influence of the number of landmarks on the co-variation analyses. The subsampling was performed by decimating the sliding-semilandmarks uniformly for each articulation in order to obtain a conformation of landmarks homogenously distributed in each articulation. To do so, we decimated the landmarks for each bone for a single specimen using the function 'uniform sample' in Geomagic Studio. Then, the operation is reiterated allowing us to obtain each bone of each specimen uniformly subsampled in the same way. Ultimately this procedure resulted in four data sets, which are as follows.

Table 3 Definition of the landmarks of the ulna used for geometric morphometrics analyses.

Landmark	Definition
1*	Most lateral point of contact between the trochlear notch and the radial notch
2*	Most proximo-lateral point of the incisure of the trochlear notch
3*	Point of maximum of concavity of the proximal part of the trochlear notch
4*	Most proximo-medial point of the incisure of the trochlear notch
5*	Most palmo-lateral point of olecranon process
6*	Most palmo-medial point of olecranon process
7*	Most dorso-medial point of olecranon process
8*	Most dorso-lateral point of olecranon process
9*	Point where the most medial part of the coronoid process meets the most medio-distal part of the trochlear notch
10*	Most anterior point of contact between the trochlear notch and the radial notch
11*	Point of maximum of concavity between the radial notch and the trochlear notch
12*	Most latero-distal point of insertion of the radial notch
13	Tip of the styloid process
14	Most distal point of the articular facet that articulates with the radius
15	Most proximal point of the articular facet that articulates with the radius
16*	Point where the proximo-lateral part of the coronoid process meets the lateral part of the trochlear notch
17	Most distal point of insertion of the medial epicondylar crest on the diaphysis
18	Point of maximum of curvature of the medial epicondylar crest
19	Most proximal point of insertion of the medial epicondylar crest on the diaphysis

*Represents landmarks used for the surface analyses of the elbow articulation.

Table 4 Definition of the landmarks of the radius used for geometric morphometrics analyses.

Landmark	Definition
1*	Most disto-lateral point of anterior side of the ulnar facet
2*	Most proximo-lateral point of anterior side of the ulnar facet
3*	Point of maximum of concavity of the anterior part of the fovea
4*	Tip of the fovea
5	Most disto-medial point of the distal articular facet with the ulna
6	Most proximal point of curvature of the distal articular facet with the ulna
7	Most disto-lateral point of the distal articular facet with the ulna
8	Distal tip of the styloid process
9	Medial tip of the styloid process
10	Most disto-lateral point of the dorsal side of the radius
11	Most proximal point of the groove for extensor digitorum and extensor indicis
12	Most proximal point of groove for extensor carpi radialis longus and brevis
13*	Most disto-medial point of the anterior side of the ulnar facet

*Represents landmarks used for the surface analyses of the elbow articulation.

1 The entire forelimb dataset with 303 landmarks (21 homologous landmarks and 282 sliding-semilandmarks) for the humerus, 165 landmarks (13 homologous landmarks and 152 sliding-semilandmarks) for the radius and 330 landmarks (19 homologous landmarks and 311 sliding-semilandmarks) for the ulna, allowing us to describe the shape of each bone and more precisely their articulations (Fig. 3).

2 The forelimb dataset after uniformly subsampling the number of sliding-semilandmarks to 50 landmarks (21 homologous landmarks and 29 sliding-semilandmarks) for the humerus, 50 landmarks (13 homologous landmarks and 37 sliding-semilandmarks) for the radius and 50 landmarks (19 homologous landmarks and 31 sliding-semilandmarks) for the ulna.

3 The elbow dataset with 300 landmarks on the distal part (15 homologous landmarks and 285 sliding-semilandmarks) of the humerus, 144 landmarks (5 homologous landmarks and 139 sliding-semilandmarks) on the proximal part of the radius and 287 landmarks (13 homologous landmarks and 274 sliding-semilandmarks) on the proximal part of the ulna, describing only the shape of the distal articulations of the humerus and the proximal articulations of the ulna and radius.

4 The elbow dataset composed of the data representing the distal part of the humerus, the proximal part of the ulna and the proximal part of the radius after uniformly subsampling to 50 landmarks on the distal part (15 homologous landmarks and 35 sliding-semilandmarks) of the humerus, 50 landmarks (five homologous landmarks and 45 sliding-semilandmarks) on the proximal part of the radius and 50 landmarks on the proximal part (13 homologous landmarks and 37 sliding-semilandmarks) of the ulna.

Study of the co-variation of two structures using 2B-PLS

To quantify shape co-variation and the morphological integration between each of the long bones of the forelimb, we performed 2B-PLS approaches (Rohlf & Corti, 2000) implemented in the library Rmorph (Baylac, 2012) for each data set separately. This method allows us to study shape co-variation between humerus and radius, humerus and ulna, and ulna and radius. A covariance matrix is calculated from two blocks representing the shape variation of the two objects (humerus–radius, humerus–ulna and ulna–radius). 2B-PLS operations generate a pair of vectors (or axes) for each block. Thus, patterns of covariance between two blocks (humerus–radius, humerus–ulna and ulna–radius) can be explored, and the PLS axis can be plotted, helping us to understand the co-variation

between the long bones of the forelimb. Finally, a PLS coefficient is calculated allowing to estimate the degree of morphological integration. Its significance is calculated by comparing the singular value to those obtained from permuted blocks. The PLS coefficient was calculated using the function morphol.integr in R using the Geomorph library (Adams & Otárola-Castillo, 2013) following the method PLS (Bookstein et al. 2003). This function uses the 3D landmark data after superimposition and performed an analysis that is referred to as singular warps analysis (Bookstein et al. 2003). A significance test is obtained by 10 000 permutations of the landmarks in one block relative to those in the other. Then a histogram of coefficients is obtained by resampling. The P_{95}-value is calculated by comparison of the observed PLS coefficient to those obtained after resampling. The significance of each linear combination is assessed by comparing the singular value (PLS coefficient) with those obtained from permuted blocks. If the PLS coefficient was higher than those obtained from permutated blocks, then its associated P_{95}-value is considered as significant.

Testing the morphological integration using the RV-coefficient

To statistically assess the significance and the magnitude of shape co-variation between each of the long bones of the forelimb, we performed an RV test in R (Escoufier, 1973; Klingenberg, 2009) using the function morphol.integr in the Geomorph library (Adams & Otárola-Castillo, 2013) following the method RV. The RV-coefficient allows in complement to the PLS coefficient to represent the strength of co-variation between two structures, and provides a value ranging between 0 and 1 (Goswami & Polly, 2010). This coefficient is more analogous to a correlation coefficient. Its calculation mainly involves the division of the covariance between the two sets of variables by the variance of each data set or block. When the RV-coefficient is 0, no co-variation between structures is present; when the RV-coefficient is 1, the two structures are perfectly integrated, which means that the co-variations between the two structures are higher. To estimate the degree of morphological integration, we compared the RV-coefficient estimated from 10 000 permutations of the landmarks in one data matrix relative to those in the other for each hypothesis. Then, the results are presented as a histogram that represents coefficients obtained via re-sampling of the observed value. A *P*-value (significance level = 0.001) is associated and allows one to assess the significance level of the observed signal (Escoufier, 1973; Klingenberg, 2009). The *P*-value is calculated by comparison of the observed RV-coefficient to those obtained after resampling. If the RV-coefficient was higher than those obtained from permutated blocks resampling, then its associated *P*-value is considered as significant.

Results

Co-variation and morphological integration of the entire forelimb

Humerus and radius

The first PLS axis described 98.3% of the total shape co-variation between the humerus and the radius (Fig. 4a). The PLS coefficient is 0.89 and its associated permutation test is significant ($P \ll 0.001$), which indicates strong co-variation between the humerus and the radius.

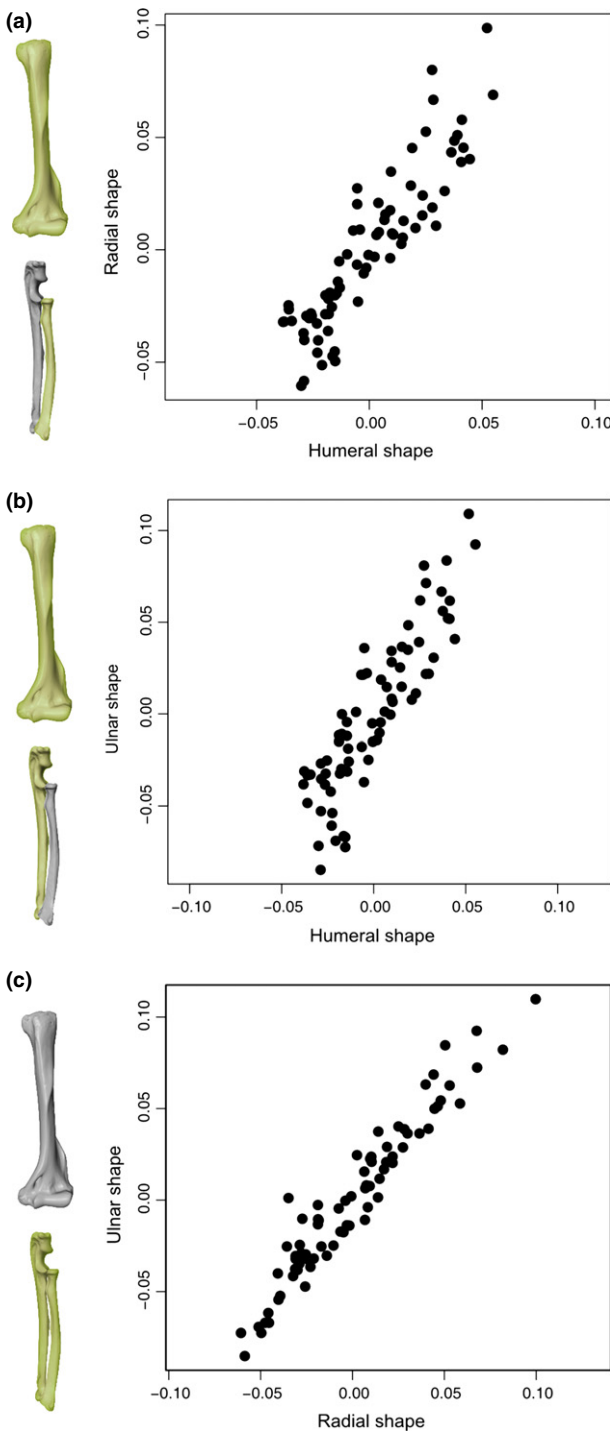

Fig. 4 Scatter plot of the first PLS axis describing: (a) 98.3% of the total shape co-variation between the humerus and the radius; (b) 96.8% of the total shape co-variation between the humerus and the ulna; (c) 98.5% of the total shape co-variation between the radius and the ulna.

The RV-coefficient (Fig. S1a) is 0.77, and its associated test is significant ($P \ll 0.001$), which means that there is a strong morphological integration between the humerus and the

radius. The results for the shape co-variation between the humerus and radius after subsampling of the data set (Fig. S2a) are very similar to those obtained when using the full data set (97.5% of the total shape co-variation, PLS coefficient = 0.87, $P \ll 0.001$; RV-coefficient = 0.72, $P \ll 0.001$), indicating that the results are robust (Fig. S3a).

Humerus and ulna

The first PLS axis between the humerus and the ulna described 96.8% of total shape co-variation (Fig. 4b). The PLS coefficient is 0.87 and its associated permutation test is significant ($P \ll 0.001$), which indicates co-variation between the humerus and the ulna.

The RV-coefficient (Fig. S1b) is 0.73, and its associated statistical test ($P \ll 0.001$) shows that there is morphological integration between the humerus and the ulna. The results of the analysis of the shape co-variation between the humerus and ulna after subsampling (Fig. S2b) are again very similar to those obtained for the full data set (95% of the total shape co-variations, PLS coefficient = 0.85, $P \ll 0.001$; RV-coefficient = 0.67, $P \ll 0.001$; Fig. S3b).

Radius and ulna

The first PLS axis described 98.5% of the total shape co-variation between the radius and the ulna (Fig. 4c). The PLS coefficient is 0.96 and its associated permutation test is significant ($P \ll 0.001$), indicating strong co-variation between the radius and the ulna.

The RV-coefficient (Fig. S1c) is 0.90 and its associated statistical test ($P \ll 0.001$) shows that there is a very strong morphological integration between the radius and the ulna. The results of the analysis of shape co-variation between the radius and the ulna after subsampling (Fig. S2c) are again similar to those obtained when using the full data set (97% of the total shape co-variations, PLS coefficient = 0.96, $P \ll 0.001$; RV-coefficient = 0.87, $P \ll 0.001$; Fig. S3c).

Co-variation and morphological integration at the elbow joint

Distal articulation of the humerus and proximal articulation of the radius

The first PLS axis described 46.6% of the total shape co-variation (Fig. 5a) between the humerus and the radius. The PLS coefficient is 0.73 and its associated permutation test is significant ($P \ll 0.001$), which indicates co-variation between the humerus and radius.

The RV-coefficient (Fig. S4a) is 0.31 and its associated statistical test ($P \ll 0.001$) is significant, showing that there is morphological integration between the humerus and radius. The results of the analysis of shape co-variation between the humerus and the radius after subsampling (Fig. S5a) are again very similar (44.4% of the total shape co-variations, PLS coefficient = 0.78, $P \ll 0.001$), and show

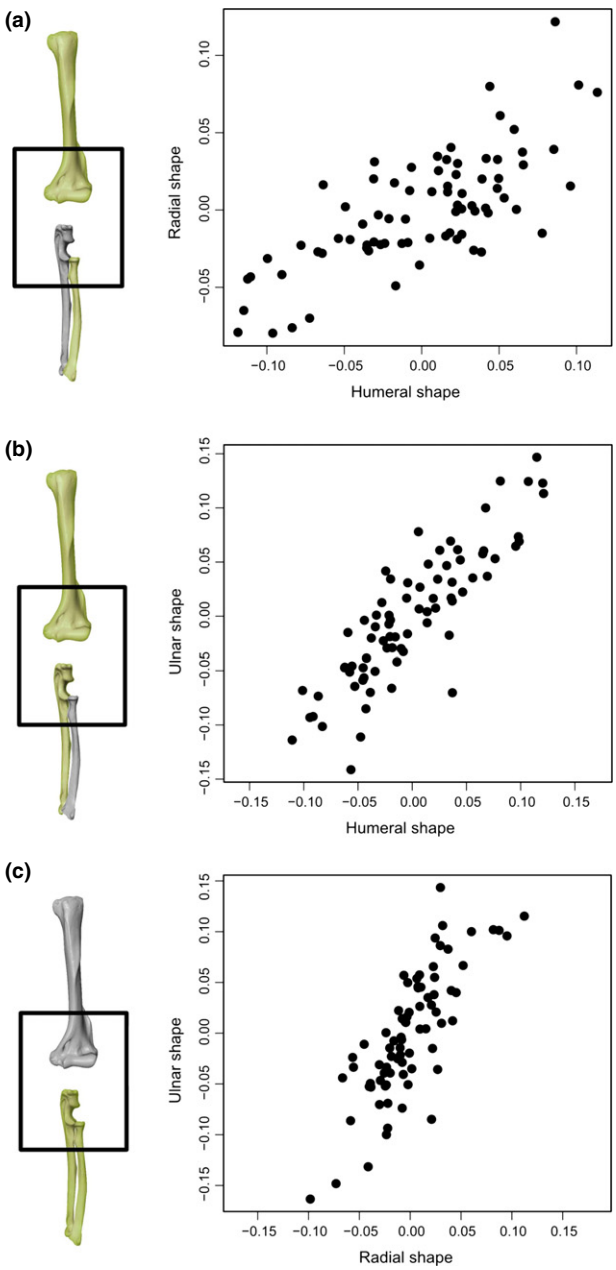

Fig. 5 Scatter plot of the first PLS axis describing: (a) 46.6% of the total shape co-variation between the distal part of the humerus and the proximal part of the radius; (b) 54% of the total shape co-variation between the distal part of the humerus and the proximal part of the ulna; (c) 45.7% of the total shape co-variation between the proximal part of the radius and the ulna.

that both humerus and radius are morphologically integrated (RV-coefficient = 0.34, $P \ll 0.001$; Fig. S6a).

Distal articulation of the humerus and proximal articulation of the ulna

The first PLS axis described 54% of the total shape co-variation between the humerus and the ulna (Fig. 5b). The PLS coefficient is 0.86 and its associated permutation test is

significant ($P \ll 0.001$), which indicates a strong co-variation between the humerus and the ulna.

The RV-coefficient is 0.59 (Fig. S4b) and its associated statistical test ($P \ll 0.001$) is significant, and shows that there is strong morphological integration between both humerus and ulna. The results of the analysis of shape co-variation between the humerus and the ulna after subsampling (Fig. S5b) are somewhat different (39% of the total shape co-variations; PLS coefficient = 0.83, $P \ll 0.001$), but still demonstrate a strong morphological integration (Fig. S6b) between both bones (RV-coefficient = 0.51, $P \ll 0.001$).

Proximal articulations of the radius and the ulna

The first PLS axis described 45.7% of the total shape co-variation between the radius and the ulna (Fig. 5c). The PLS coefficient is 0.79 and its associated permutation test is significant ($P \ll 0.001$), which indicates a strong co-variation between the radius and the ulna.

The RV-coefficient is 0.37 (Fig. S4c) and its associated statistical test ($P \ll 0.001$) is significant, and shows that there is a morphological integration between radius and ulna. The results of the analysis of shape co-variation between the radius and ulna after subsampling (Fig. S5c) are quite similar to those obtained for the full data set (42.8% of the total shape co-variation, PLS coefficient = 0.77, $P \ll 0.001$) and also demonstrate strong morphological integration between both bones (RV-coefficient = 0.37, $P \ll 0.001$; Fig. S6c).

Discussion

Influence of the number of landmarks

Interestingly, our results show that varying the number of landmarks used to describe the shape of the bones in our study did not significantly influence the results. Indeed, the results of the morphological integration analyses for the forelimb (Figs 4 and S2) and the elbow joint (Figs 5 and S5) are similar before and after subsampling down to 50 landmarks for each element. Furthermore, the results of the calculation of the associated RV-coefficients for the whole forelimb (Figs S1 and S3) and the elbow joint (Figs S4 and S6) are also very similar before and after subsampling. This suggests that the number of landmarks does not strongly influence the result of our analyses of co-variance and morphological integration. Increasing the number of landmarks, albeit significantly increasing the accuracy of the shape description, thus does not alter the results. Nevertheless, there is a difference concerning the results for the co-variation of the distal part of the humerus and the proximal part of the ulna before and after subsampling (Figs 5b and S5b). This difference may be due to the number of points, which decreases considerably for these two structures after the subsampling in comparison to those of the other structures examined.

Co-variation and morphological integration of the long bones of the forelimb

Our results show that there is more shape co-variation between the long bones of the lower arm (radius and ulna) than between bones of the upper arm and lower arm (humerus and radius; humerus and ulna; Fig. 4). These results are further supported by the strong morphological integration measured between the bones of the forearm (Fig. S1). This high morphological integration is possibly the result of the fact that the radius and the ulna need to interact functionally to allow rotation of the radius relative to the ulna and have two joints in common (Rose, 1988, 1993; Argot, 2001, 2003; Patel, 2005). These pronation–supination movements play an important role during many behaviours of an animal, including locomotion, grasping, mating and hunting (Gonyea, 1978; Rose, 1988, 1993; Iwaniuk et al. 1999; Argot, 2001, 2003; Fabre et al. 2013b). As such, functional constraints on the mobility of the lower arm appear to be driving the co-evolution of the radius and ulna. Moreover, these results suggest that functional units are identical to developmental ones given the fact that the radius and ulna share a similar developmental pathway (Wellik & Capecchi, 2003; Young & Hallgrímsson, 2005; Schmidt & Fischer, 2009; Young et al. 2010). Indeed, *Hox 11* is expressed during the development of both the radius and ulna, but not the humerus (Fig. 2). The humerus, on the other hand, despite showing strong functional co-variation with the long bones of the lower arm, is subjected to additional constraints, and has, as shown by other studies (Wellik & Capecchi, 2003; Young & Hallgrímsson, 2005; Goswami et al. 2009; Schmidt & Fischer, 2009; Young et al. 2010; Bell et al. 2011; Bennett & Goswami, 2011), an independent developmental origin with the unique expression of *Hox 9*. Moreover, it interacts functionally with the shoulder girdle proximally, which places independent and different demands on its morphology (Rose, 1988, 1993; Argot, 2001, 2003; Patel, 2005).

Co-variation and the degree of morphological integration at the elbow joint

In agreement with our prediction, our results show that shape co-variations are stronger between the distal part of the humerus and the proximal part of the ulna than between the distal part of the humerus and the proximal part of the radius. Moreover, the co-variation between the proximal part of the ulna and that of the radius is lower (Figs 5 and S4). This suggests that the stability of the elbow joint, which is mainly conferred by the interaction between the humerus and ulna (Rose, 1988, 1993; Argot, 2001, 2003; Patel, 2005), drives much of the co-evolution between the forelimb elements involved in this joint. Stability is important at this level, because the joint needs to limit displacement of the ulna relative to the radius in addition to

transferring the load from upper to lower limb as imposed by gravity, locomotion and other behaviours (Rose, 1988, 1993; Argot, 2001, 2003; Patel, 2005; Fabre et al. 2013a,b). Furthermore, this stronger co-variation can be explained by the fact that the ulna is deeply interlocked with the humerus, and as such shares a bigger surface in common with the distal articulation of the humerus than the humerus does with the radius or the radius with the ulna. In contrast, mobility, which we here mainly refer to as the motion occurring at the humero-radial (flexion–extension) and radio-ulnar joints, (pronation–supination) induces a lower co-variation (Rose, 1988). This highlights the importance of the distal articulation of both radius and ulna in allowing the mobility of the forearm. These results show that at the level of the elbow joint, stability is important and seems to impose stronger constraints on the morphology of the elbow joint, thus driving the strong functional co-variation observed at the humero-ulnar joint.

Concluding remarks

Our results largely confirm our predictions and show that morphological integration is stronger for long bones that form functional units whose role is crucial in the adaptations to locomotor mode and lifestyle of the animals studied. Depending on the level of investigation (elbow vs. entire arm), different results are obtained suggesting that the functional unit of the lower arm is comprised of the entire radius and ulna. Yet, at the level of the elbow the critical functional unit appears to be the articulation between humerus and ulna providing the stability of the joint and subsequently allowing the movement of the radius across the ulna. Future studies exploring shape variation and morphological integration at the elbow among other species are needed to test the generality of the observed results. Exploring patterns of co-variation in a group of closely related species including cursorial Carnivora that have lost the ability to supinate their paws (Ewer, 1973; Andersson & Werdelin, 2003; Andersson, 2004; Van Valkenburgh, 2007), but also quadrupedal vs. bipedal species, such as primates, would be of interest as it would allow us to understand whether the elbow in bipedal species is free from constraints on stability (i.e. loss of the strong degree of co-variation between humerus and ulna) as would be predicted by our data.

Acknowledgements

The authors thank J. Cuisin, G. Véron, J. Villemain and C. Bens for access to specimens from the collections Mammifères et Oiseaux, MNHN, Paris; L. Costeur, from the Naturhistorisches Museum, Basel; J. Chupasko from the Harvard Museum of Comparative Zoology, Cambridge, Massachusetts; and S. Peurach from the Smithsonian National Museum of Natural History, Washington, District of Columbia for allowing us to scan the material. The authors thank the 'plate-forme de morphométrie' of the UMS 2700 (CNRS, MNHN) for access to the surface scanner. A.-C. Fabre thanks the doctoral school FdV, the Fondation Bettencourt-Schueller, and A. Murray and M. Collins in helping her to obtain a UCL IMPACT scholarship for funding. The authors also thank L. Bascher, F. Goussard, M. Randau, S. Moulin and C. Houssin for their helpful discussions and comments on this manuscript, and two anonymous reviewers for constructive comments on an earlier version of the paper.

Conflict of interest

The authors declare no conflict of interest.

Author contributions

A.C.F. conceived the paper, performed the data acquisition and analysis, and drafted the manuscript. R.C. helped conceive the paper and helped with data analysis. A.G. and S.P. helped design the study, and all authors contributed to the writing of the manuscript.

References

Adams DC, Otárola-Castillo E (2013) Geomorph: an R package for the collection and analysis of geometric morphometric shape data. *Methods Ecol Evol* **4**, 393–399.

Andersson K (2003) *Locomotor Evolution in the Carnivora (Mammalia): Evidence from the Elbow Joint*. Sweden: University of Uppsala.

Andersson K (2004) Elbow-joint morphology as a guide to forearm function and foraging behaviour in mammalian carnivores. *Zool J Linn Soc* **142**, 91–104.

Andersson K (2005) Were there pack-hunting canids in the Tertiary, and how can we know? *Paleobiology* **31**, 56–72.

Andersson K, Werdelin L (2003) The evolution of cursorial carnivores in the tertiary: implications of elbow-joint morphology. *Proc Biol Sci* **270**, S163–S165.

Argot C (2001) Functional-adaptive anatomy of the forelimb in the Didelphidae, and the paleobiology of the Paleocene marsupials *Mayulestes ferox* and *Pucadelphys andinus*. *J Morphol* **247**, 51–79.

Argot C (2003) Functional adaptations of the postcranial skeleton of two Miocene Borhyaenoids (Mammalia, Metatheria), *Borhyaena* and *Prothylacinus*, from South America. *Palaeontology* **46**, 1213–1267.

Baylac M (2012) Rmorph: an R geometric and multivariate morphometrics library.

Bell E, Andres B, Goswami A (2011) Limb integration and dissociation in flying vertebrates: a comparison of birds, bats, and pterosaurs. *J Evol Biol* **24**, 2586–2599.

Bennett CV, Goswami A (2011) Does reproductive strategy drive limb integration in marsupials and monotremes? *Mamm Biol* **76**, 79–83.

Bookstein FL (1991) *Morphometric Tools for Landmark Data: Geometry and Biology*. New York: Cambridge University Press.

Bookstein FL (1997) Landmark methods for forms without landmarks: morphometrics of group differences in outline shape. *Med Image Anal* **1**, 225–243.

Bookstein FL, Green WDK (2002) Users Manual, EWSH3.19. Available at: http://brainmap.stat.washington.edu/edgewarp/ (accessed 29 April 2014).

Bookstein FL, Gunz P, Mitteroecker P, et al. (2003) Cranial integration in Homo: singular warps analysis of the midsagittal plane in ontogeny and evolution. *J Hum Evol* **44**, 167–187.

Candela A, Picasso M (2008) Functional anatomy of the limbs of Erethizontidae (Rodentia, Caviomorpha): indicators of locomotor behavior in Miocene porcupines. *J Morphol* **269**, 552–593.

Cheverud J (1982) Phenotypic, genetic, and environmental morphological integration in the cranium. *Evolution* **36**, 499–516.

Eizirik E, Murphy WJ, Koepfli K-P, et al. (2010) Pattern and timing of diversification of the mammalian order Carnivora inferred from multiple nuclear gene sequences. *Mol Phylogenet Evol* **56**, 49–63.

Escoufier Y (1973) Le traitement des variables vectorielles. *Biometrics* **29**, 751–760.

Ewer RF (1973) *The Carnivores*. Ithaca, NY: Cornell University Press.

Fabre A-C, Cornette R, Peigné S, et al. (2013a) Influence of body mass on the shape of forelimb in musteloids carnivorans. *Biol J Linn Soc* **110**, 91–103.

Fabre A-C, Cornette R, Slater G, et al. (2013b) Getting a grip on the evolution of grasping in musteloid carnivorans: a three-dimensional analysis of forelimb shape. *J Evol Biol* **26**, 1521–1535.

Flores DA, Diaz MM (2009) Postcranial skeleton of *Glironia venusta* (Didephimorphia, Didelphidae, Caluromyinae): description and functional morphology. *Zoosyst Evol* **85**, 311–339.

Gonyea WJ (1978) Functional implications of felid forelimb morphology. *Acta Anat* **102**, 111–121.

Goswami A, Polly PD (2010) Methods for studying morphological integration, modularity and covariance evolution. In: *Quantitative Methods in Paleobiology*, (eds Alroy J, Hunt G), pp. 213–243. Paleontological Society Short Course, October 30th, 2010. *The Paleontological Society Papers* Volume 16.

Goswami A, Weisbecker V, Sánchez-Villagra MR (2009) Developmental modularity and the marsupial-placental dichotomy. *J Exp Zool B Mol Dev Evol* **312B**, 186–195.

Gunz P, Mitteroecker P (2013) Semilandmarks: a method for quantifying curves and surfaces. *Hystrix* **24**, 1–7.

Gunz P, Mitteroecker P, Bookstein FL (2005) Semilandmarks in three dimensions. In: *Modern Morphometrics in Physical Anthropology* (ed. Slice D), pp. 73–98. New York: Plenum Press.

Gunz P, Mitteroecker P, Neubauer S, et al. (2009) Principles for the virtual reconstruction of hominin crania. *J Hum Evol* **57**, 48–62.

Halenar LB (2011) Reconstructing the locomotor repertoire of *Protopithecus brasiliensis.* I. Body size. *Anat Rec (Hoboken)* **294**, 2024–2047.

Hallgrímsson B, Jamniczky H, Young NM, et al. (2009) Deciphering the palimpsest: studying the relationship between morphological integration and phenotypic covariation. *Evol Biol* **36**, 355–376.

Iwaniuk AN, Pellis SM, Whishaw IQ (1999) The relationship between forelimb morphology and behaviour in North American carnivores (Carnivora). *Can J Zool* **77**, 1064–1074.

Klingenberg CP (2008) Morphological integration and developmental modularity. *Annu Rev Ecol Evol Syst* **39**, 115–132.

Klingenberg CP (2009) Morphometric integration and modularity in configurations of landmarks: tools for evaluating *a priori* hypotheses. *Evol Dev* **11**, 405–421.

MacLeod N, Rose KD (1993) Inferring locomotor behavior in Paleogene mammals via eigenshape analysis. *Am J Sci* **293-A**, 300–355.

Milne N, Vizcaíno SF, Fernicola JC (2009) A 3D geometric morphometric analysis of digging ability in the extant and fossil cingulate humerus. *J Zool* **278**, 48–56.

Mitteroecker P, Gunz P (2009) Advances in geometric morphometrics. *Evol Biol* **36**, 235–247.

Nowak RM (2005) *Walker's Carnivores of the World*. Baltimore: The Johns Hopkins University Press.

Olson EC, Miller RL (1958) *Morphological Integration*. Chicago, IL: University of Chicago Press.

Parr WCH, Wroe S, Chamoli U, et al. (2012) Toward integration of geometric morphometrics and computational biomechanics: new methods for 3D virtual reconstruction and quantitative analysis of Finite Element Models. *J Theor Biol* **301**, 1–14.

Patel BA (2005) The hominoid proximal radius: re-interpreting locomotor behaviors in early hominins. *J Hum Evol* **48**, 415–432.

R Development Core Team (2012) *R: A Language and Environment for Statistical Computing. R Foundation for Statistical Computing*. Vienna: R Foundation for Statistical Computing.

Rohlf FJ, Corti M (2000) Use of two-block partial least-squares to study covariation in shape. *Syst Biol* **49**, 740–753.

Rohlf FJ, Slice DE (1990) Extensions of the procrustes method for the optimal superimposition of landmarks. *Syst Zool* **39**, 40–59.

Rose MD (1988) Another look at the anthropoid elbow. *J Hum Evol* **17**, 193–224.

Rose MD (1993) Functional anatomy of the elbow and forearm in primates. In: *Postcranial Adaptations in Non-Human Primates*. (ed. Gebo DL), pp. 70–95. DeKalb: Northern Illinois University Press.

Sato JJ, Wolsan M, Minami S, et al. (2009) Deciphering and dating the red panda's ancestry and early adaptive radiation of Musteloidea. *Mol Phylogenet Evol* **53**, 907–922.

Sato JJ, Wolsan M, Prevosti FJ, et al. (2012) Evolutionary and biogeographic history of weasel-like carnivorans (Musteloidea). *Mol Phylogenet Evol* **63**, 745–757.

Schmidt M, Fischer MS (2009) Morphological integration in mammalian limb proportions: dissociation between function and development. *Evolution* **63**, 749–766.

Schutz H, Guralnick R (2007) Postcranial element shape and function: assessing locomotor mode in extant and extinct mustelid carnivorans. *Zool J Linn Soc* **150**, 895–914.

Steiner-Souza F, De Freitas TRO, Cordeiro-Estrela P (2010) Inferring adaptation within shape diversity of the humerus of subterranean rodent *Ctenomys*. *Biol J Linn Soc* **100**, 353–367.

Van Valkenburgh B (2007) *Déjà vu*: the evolution of feeding morphology in the Carnivora. *Integr Comp Biol* **47**, 147–163.

Wellik DM, Capecchi MR (2003) *Hox10* and *Hox11* genes are required to globally pattern the mammalian skeleton. *Science* **301**, 363–367.

Wiley DF, Amenta N, Alcantara DA, et al. (2005) Evolutionary morphing. In: *Proceedings of IEEE Visualization 2005 (VIS'05), 23–28 October 2005*, Minneapolis, MN, USA.

Wilson DE, Mittermeier RA (2009) *Handbook of the Mammals of the World*. Barcelona: Lynx Edicions.

Young N, Hallgrímsson B (2005) Serial homology and the evolution of mammalian limb covariation structure. *Evolution* **59**, 2691–2704.

Young N, Wagner G, Hallgrimsson B (2010) Development and the evolvability of human limbs. *Proc Natl Acad Sci USA* **107**, 3400–3405.

Supporting Information

Additional Supporting Information may be found in the online version of this article:

Fig. S1 Histograms of the null distributions of the RV-coefficient in grey, and the RV-coefficient represented by the red arrow. **A**, the morphological integration between the humerus and the radius; **B**, the morphological integration between the humerus and the ulna; **C**, the morphological integration between the radius and the ulna.

Fig. S2 Scatter plot of the first PLS axis describing: **A**, 97.5% of the total shape co-variation between the humerus and the radius after decimation; **B**, 95% of the total shape co-variation between the humerus and the ulna after decimation; **C**, 97% of the total shape co-variation between the radius and the ulna after decimation.

Fig. S3 Histograms of the null distributions of the RV-coefficient in grey and the RV-coefficient represented by the red arrow. **A**, the morphological integration between the humerus and the radius after decimation; **B**, the morphological integration between the humerus and the ulna after decimation; **C**, the morphological integration between the radius and the ulna after decimation.

Fig. S4 Histograms of the null distributions of the RV-coefficient in grey and the RV-coefficient represented by the red arrow. **A**, the morphological integration between the distal part of the humerus and the proximal part of the radius; **B**, the morphological integration between the distal part of the humerus and the proximal part of the ulna; **C**, the morphological integration between the proximal part of the radius and the ulna.

Fig. S5 Scatter plot of the first PLS axis describing: **A**, 44.4% of the total shape co-variation between the distal part of the humerus and the proximal part of the radius after decimation; **B**, 39% of the total shape co-variation between the distal part of the humerus and the proximal part of the ulna after decimation; **C**, 42.8% of the total shape co-variation between the proximal part of the radius and the ulna after decimation.

Fig. S6 Histograms of the null distributions of the RV-coefficient in grey and the RV-coefficient represented by the red arrow. **A**, the morphological integration between the distal part of the humerus and the proximal part of the radius after decimation; **B**, the morphological integration between the distal part of the humerus and the proximal part of the ulna after decimation; **C**, the morphological integration between the proximal part of the radius and the ulna after decimation.

Table S1 Specimens used in the analyses. Institutional abbreviations are as follows: CG, Muséum National d'Histoire Naturelle Catalogue Générale, Paris; MCZ, Harvard Museum of Comparative Zoology, Cambridge, Massachusetts; NMB, Natuhistorishes Museum Basel, Basel; USNM, the Smithsonian National Museum of Natural History, Washington, District of Columbia. Sex abbreviations are follows: F: female; M: male; U: unknown.